

Kinetic mechanism for modeling of electrochemical reactions

Petr Červenka, Jiří Hrdlička, Michal Příbyl, and Dalimil Šnita

Department of Chemical Engineering, Institute of Chemical Technology, Prague, Technická 5, 166 28 Praha 6, Czech Republic

(Received 24 March 2011; revised manuscript received 6 October 2011; published 25 April 2012)

We propose a kinetic mechanism of electrochemical interactions. We assume fast formation and recombination of electron donors \mathcal{D}^- and acceptors \mathcal{A}^+ on electrode surfaces. These mediators are continuously formed in the electrode matter by thermal fluctuations. The mediators \mathcal{D}^- and \mathcal{A}^+ , chemically equivalent to the electrode metal, enter electrochemical interactions on the electrode surfaces. Electrochemical dynamics and current-voltage characteristics of a selected electrochemical system are studied. Our results are in good qualitative agreement with those given by the classical Butler-Volmer kinetics. The proposed model can be used to study fast electrochemical processes in microsystems and nanosystems that are often out of the thermal equilibrium. Moreover, the kinetic mechanism operates only with the surface concentrations of chemical reactants and local electric potentials, which facilitates the study of electrochemical systems with indefinable bulk.

DOI: [10.1103/PhysRevE.85.041505](https://doi.org/10.1103/PhysRevE.85.041505)

PACS number(s): 82.45.Gj, 05.45.-a, 82.45.Fk, 82.45.Hk

I. INTRODUCTION

Electrochemical interactions play an important role in many fields of science and industry. The energy storage and release in battery technology or fuel cell technology are among the most important scopes [1–3]. Reversible electrochemical cells such as rechargeable batteries [4–6] can be used either for the production of electric energy from an electrochemical reaction or in the reverse electrolytic mode. Electrochemical reactions in the field of corrosion science also constitute one of the fundamental problems [7,8]. Faradaic reactions are principal phenomena in micropumps driven by an electric field [9–12], galvanic cells intended for metal deposition [13], or electroseparation applications [14]. Problems emerge in microelectrochemical systems because traditional macroscopic approximations such as electroneutrality or thermal equilibrium often are not valid due to small dimensions, large applied voltages, and a high rate of transport processes. The relative importance of surface phenomena also increases with miniaturization.

The theoretical study of electrochemical reactions was initially performed by Gruz and Volmer [15]. The reaction rate was expressed as a function of concentrations of reactants and an actual value of electrode potential, which is the difference between the inner (Galvani) electric potential on the metal surface and the electric potential in an electrolyte bulk. The Butler-Volmer (BV) equation does not take into account processes in the compact (Stern) and diffuse (Debye) parts of an electrical double layer (EDL) (Fig 1). Frumkin [16] later modified the classical BV description. He considered that the rate of electrochemical reaction depends on the electric potential difference across the compact layer. It is assumed that the charge transfer occurs at some atomic distance away from the electrodes, at a reaction plane (the outer Helmholtz plane), where the electroactive species can react. The electrochemical methods that use the BV equation (or the Tafel linearized equation) for the evaluation of kinetic parameters of electrochemical reactions are electrochemical impedance spectroscopy [17–19] and potential-relaxation methods [20,21].

Several theoretical studies of transport processes in microsystems with Faradaic interactions have been published

[22–29]. The analysis of these systems is based on the solution of the Poisson-Nernst-Planck (PNP) equations. The governing PNP equations were combined with the Frumkin correction of the classical BV kinetics. This approach allows one to study the transport processes in the diffuse layer together with electrochemical processes; however, it is not derived from the character of reaction mechanism. With the growing importance of various microfluidic and nanofluidic electrochemical sensors, electro-osmotic pumps, and dielectrophoretic sorters (often operating under high frequencies) [30–32], there is a serious need to develop an alternative description for systems out of thermal equilibrium. Even if the Frumkin modification of the BV kinetics is used, it still assumes the Boltzmann distribution of ions at electrode interfaces [9,33], which is simply not true in many high-frequency electrochemical systems.

II. ELECTROCHEMICAL SYSTEM

Here we study a reversible electrochemical reaction with one electron transfer



The BV approach considers that the chemical energy barrier for the reaction and movement of ions through the EDL is reduced by the electrostatic energy $\alpha F \Delta \phi$. The parameter α is called a charge-transfer coefficient. The basic description of the intensity of charge transfer can be expressed as

$$i = F \left[k_O c_A^b \exp \left(\frac{(1-\alpha)F\Delta\phi}{RT} \right) - k_R c_{A^+}^b \exp \left(\frac{-\alpha F\Delta\phi}{RT} \right) \right], \quad (2)$$

where i , F , R , T , and $\Delta\phi$ are the electric current density, the Faraday constant, the molar gas constant, the absolute temperature, and the electric potential difference across the EDL, respectively (see Table I). The symbols k_O and k_R represent the oxidation and reduction kinetic rate constants, respectively, and $c_{A^+}^b$ and c_A^b are the bulk concentrations.

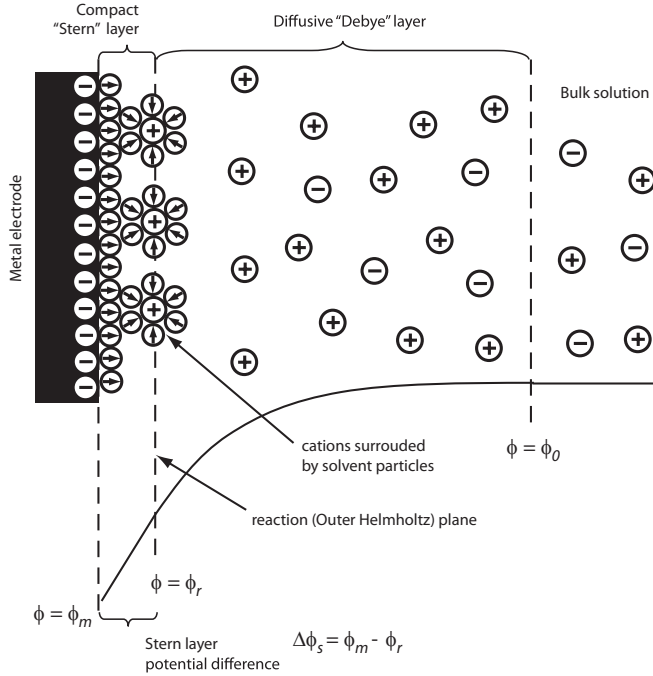


FIG. 1. Scheme of electric potential profile across the electric double layer.

The Frumkin modification [16] of Eq. (2) is

$$i = F \left[k'_O c_A \exp \left(\frac{(1 - \alpha) \Delta \phi_S F}{RT} \right) - k'_R c_{A^+} \exp \left(\frac{-\alpha \Delta \phi_S F}{RT} \right) \right], \quad (3)$$

where k'_O and k'_R are the modified oxidation and reduction kinetic rate constants. The Frumkin modification takes into account the fact that the concentrations at the outer Helmholtz plane (c_{A^+} , c_A) significantly differ from those in the electrolyte bulk ($c_{A^+}^b$, c_A^b). The symbol $\Delta \phi_S$ denotes the electric potential difference across the Stern layer (see Fig. 1 for the EDL structure).

In this paper we suggest an alternative kinetic model of the Faradaic reactions. The scheme of an electrochemical cell arrangement is outlined in Fig. 2. We consider that a dilute electrolyte consists of a reactive metal cation A^+ and inert ions B^- and C^+ that do not participate in electrode reactions. When electrodes made from metal A are immersed in the electrolyte that is free of A^+ ions, metal A is oxidized and A^+ ions are then released into the electrolyte. This transient

TABLE I. List of constants.

Symbol	Quantity	Value
F	Faraday constant (C mol ⁻¹)	96485
R	molar gas constant (J K ⁻¹ mol ⁻¹)	8.3145
T	temperature (K)	298.15
ϵ	electrolyte permittivity (F m ⁻¹)	6.954×10^{-10}
c_0	electrolyte concentration (mol m ⁻³)	1
λ_D	Debye length (m)	9.619×10^{-9}
D	diffusivity (m ² s ⁻¹)	2×10^{-9}

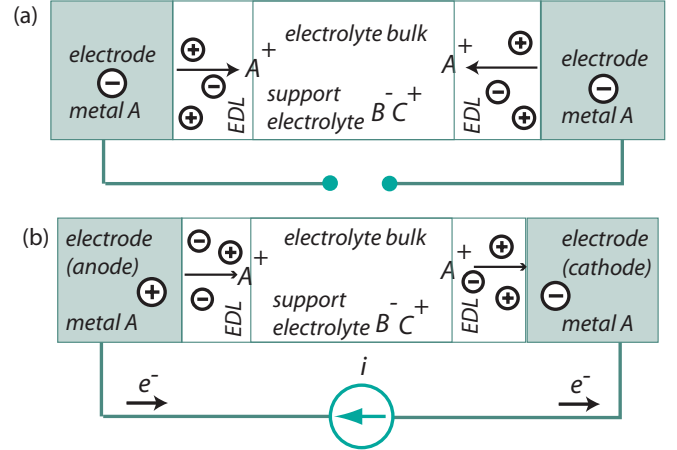
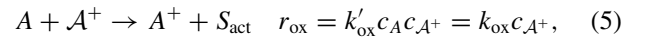
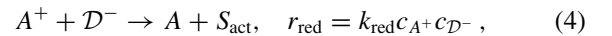


FIG. 2. (Color online) Scheme of an electrochemical cell: (a) transient processes when electrodes are immersed in an electrolyte and (b) cell under a current load.

dissolution of the electrodes continues until an electrochemical equilibrium is established (given by the Nernst equation). Both electrodes become negatively charged [Fig. 2(a)]. If we impose an external electric field between the electrodes, the system works in the electrolysis regime [Fig. 2(b)]. At the surface of the negative electrode (cathode), the reduction of A^+ ions is the dominant electrochemical reaction. The oxidation prevails at the anode. The same amount of metal A is dissolved on the anode and deposited on the cathode in a steady state.

III. REACTION MECHANISM

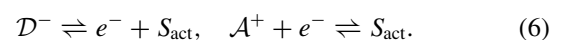
We propose the following reaction mechanism for the reduction and oxidation processes forming the overall electrochemical reaction [Eq. (1)]:



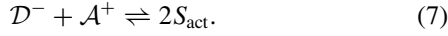
where D^- , A^+ , and S_{act} denote the donor of electrons, the acceptor of electrons (i.e., electron mediators), and active sites on the metal surface, respectively, and k'_{ox} and k_{red} are the reaction rate constants. The surface concentration of the metal remains approximately constant and is involved in the rate constant k_{ox} .

In this particular case (4), the metal A participates in the electrochemical reaction and simultaneously serves as a mediator (between donor and acceptor). Thus the component S_{act} is chemically equivalent to the metal A. However, in many other electrochemical reactions, A and S_{act} are different quantities. For example, the reduction of hydrogen ions on a platinum electrode (S_{act}) results in the formation of hydrogen (A).

We assume that permanent thermal fluctuations in electrode matter give rise to the formation of electron-rich atoms (donors of electrons) and electron-poor atoms (acceptors of electrons). Schematically, the process is expressed by



The formation of the donors and acceptors is considered much faster than the other reaction-transport processes (electrode reactions, diffusion, and electromigration transport in the electrolyte). Hence thermal equilibrium can be expected in the form



In this equilibrium the overall reaction rate is equal to zero and we can write

$$k_d c_{S_{\text{act}}}^2 = k_a c_{\mathcal{A}^+} c_{\mathcal{D}^-}, \quad k_d c_{S_{\text{act}}}^2 / k_a = c_{\mathcal{A}^+} c_{\mathcal{D}^-} = K_D, \quad (8)$$

where k_a , k_d , and K_D denote the donor-acceptor association rate constant, the active site dissociation rate constant, and the equilibrium constant of the donor-acceptor recombination, respectively. If there is a large surplus of active sites, their concentration can be considered constant. Alternatively, we can assume a total concentration of the active sites as a sum of concentration of the free active sites, electron donors, and electron acceptors. However, this approach brings a higher complexity to the proposed model.

The difference between concentrations of donors and acceptors on an electrode is equal to the concentration of the electric charge Q available on the electrode

$$c_{\mathcal{A}^+} - c_{\mathcal{D}^-} = Q/F \equiv 2b. \quad (9)$$

The combination of Eqs. (8) and (9) leads to explicit expressions for the concentration of donors and acceptors

$$c_{\mathcal{A}^+} = b + \sqrt{b^2 + K_D}, \quad c_{\mathcal{D}^-} = -b + \sqrt{b^2 + K_D}. \quad (10)$$

IV. MATHEMATICAL MODEL

If we assume the presence of a dilute electrolyte in the electrochemical cell, the local ion concentrations c_i are given by the molar balances

$$\frac{\partial c_i}{\partial t} = -\frac{\partial J_i}{\partial x}, \quad J_i = -D_i \frac{\partial c_i}{\partial x} - \frac{z_i D_i F}{RT} c_i \frac{\partial \phi}{\partial x}, \quad (11)$$

$$i = \mathcal{A}^+, \mathcal{B}^-, \mathcal{C}^+,$$

where the molar flux of ion J_i is given by the Nernst-Planck equation and D_i and z_i are the diffusivity and ion charge number, respectively. The distribution of the electric potential ϕ satisfies the Poisson equation

$$\frac{\partial}{\partial x} \left(\varepsilon \frac{\partial \phi}{\partial x} \right) = -q = -F \sum_i z_i c_i, \quad (12)$$

where q is the electric charge density and ε is the electric permittivity of the electrolyte (here assumed constant).

As we consider two electrodes, both made from the same material, the same boundary conditions are used for both electrode-solution interfaces. The zero molar fluxes are used for ions that do not participate in the electrode reactions. The molar flux of the reactive cation $J_{\mathcal{A}^+}$ is equal to the release or consumption via the electrochemical reactions

$$J_{\mathcal{A}^+}|_{x=0,L} = r_{\text{an,cat}} = k_{\text{ox}} c_{\mathcal{A}^+} - k_{\text{red}} c_{\mathcal{A}^+} c_{\mathcal{D}^-}. \quad (13)$$

The actual electric charge concentration Q on the electrode boundaries (where ‘‘an’’ denotes the anode at $x = 0$ and ‘‘cat’’

denotes the cathode at $x = L$) has to be evaluated in order to compute the donor and acceptor concentrations

$$\frac{\partial Q_{\text{an}}}{\partial t} \Big|_{x=0} = i - Fr_{\text{an}}, \quad \frac{\partial Q_{\text{cat}}}{\partial t} \Big|_{x=L} = -i - Fr_{\text{cat}}, \quad (14)$$

where i denotes the external electric current load, which is the principal parameter of the model. The electric potential boundary conditions are in the following form:

$$\frac{\partial \phi}{\partial x} \Big|_{x=0} = -\frac{Q_{\text{an}}}{\varepsilon}, \quad \phi|_{x=L} = 0. \quad (15)$$

Spatially uniform concentrations of \mathcal{B}^- and \mathcal{C}^+ ions and zero concentration of the reactive ion \mathcal{A}^+ are the initial condition for dynamical simulations

$$c_{\mathcal{B}^-, \mathcal{C}^+}|_{x,t=0} = c_0, \quad c_{\mathcal{A}^+}|_{x,t=0} = 0. \quad (16)$$

The model equations are transformed into a dimensionless form in the Appendix.

V. RESULTS

We first carry out dynamical simulations with zero electric current imposed on the system [Fig. 2(a)]. The metal initially dissolves due to the presence of the reactive electron acceptors in the metal layer \mathcal{A}^+ . As \mathcal{A}^+ ions are released into the electrolyte, negatively charged electron donors \mathcal{D}^- dominate on the metal electrodes due to the equilibrium, which is accompanied by the relative decrease of the electric potential (Fig. 3). As both reactants \mathcal{A}^+ and \mathcal{D}^- are now present at the electrode surface, the reverse reaction (metal deposition) becomes important. After a short period, the equilibrium state between the direct and reverse reactions is reached. The \mathcal{A}^+ concentration, the electric charge density, and the ionic strength $I_s = \frac{1}{2} \sum_i z_i^2 c_i$ attain maximal values at the electrode surfaces due to the electrostatic interaction.

A. Dynamical simulations of the electrochemical cell under a current load

Further we study the dynamical behavior of the electrochemical cell under a current load (Fig. 4). As the initial condition we used the previously obtained steady state shown in Fig. 3 (with no current load). At time $t = 0$ we quickly impose a constant electric current on the electrochemical circuit. Electrons leave the left electrode (anode) through the external circuit and the electrode becomes positively charged, i.e., more electron acceptors are available for the electrochemical reaction. This leads to the metal oxidation and release of \mathcal{A}^+ ions in the electrolyte. As the \mathcal{A}^+ ions are electrostatically repelled from the anode, the \mathcal{A}^+ concentration is significantly lower at the anode surface than in the bulk. Electrons are pumped to the right electrode (cathode), where it results in the formation of electron donors. Thus the reduction deposition of the metal becomes the favored reaction on the cathode. The \mathcal{A}^+ ions are electrostatically attracted to the cathode and then reduced. In this particular case, \mathcal{A}^+ ions are almost exhausted from the cathode vicinity due to the limited rate of the \mathcal{A}^+ ion transport.

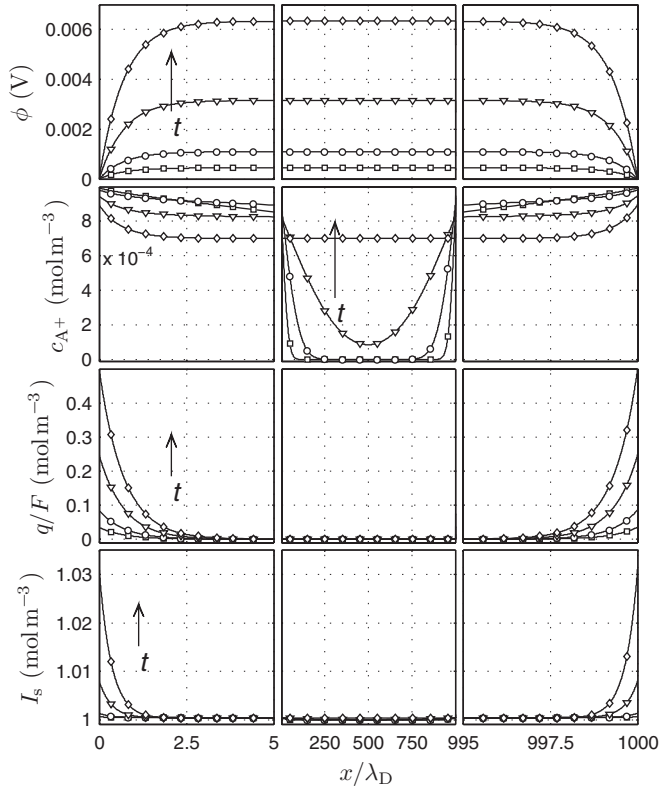


FIG. 3. Initial transient in the electrochemical cell without an electric current load. Profiles of the electric potential, A^+ concentration, electric charge density, and ionic strength are plotted. The diamond-marked profile corresponds to the achieved equilibrium. The values of the model parameters are $L = 1000\lambda_D$, $k_{\text{red}} = D/\lambda_D^2 \times 10^5 \text{ m}^3 \text{ mol}^{-1}$, $k_{\text{ox}} = D/\lambda_D^2 \times 10^2$, and $K_D = 10(c_0\lambda_D)^2$.

B. Current-voltage characteristics

In the next step we construct current-voltage (CV) characteristics of the entire electrochemical cell [Fig. 5(a)] and a half cell [Fig. 5(b)]. The term $\Delta\phi_{\text{tot}}$ in Fig. 5(a) represents the total potential difference imposed on the electrochemical cell. The anodic or cathodic overpotentials $\eta_{\text{an,cat}}$ [Fig. 5(b)] are defined as $\eta_{\text{an,cat}} = \Delta\phi_h - \Delta\phi_e$, where $\Delta\phi_h$ is the potential difference between the electrode surface and the cell center ($x = 500\lambda_D$) and $\Delta\phi_e$ is the established equilibrium electrode potential (Fig. 3).

The CV dependences of the whole electrochemical cell are characterized by exponential current growth for small potential differences. When the system becomes limited by the transport, the exponential growth is suppressed. For high potential differences, the limiting current is reached. The shift of the system from the electrochemically limited regime (exponential growth) to the transport limited regime was studied in detail. Four steady-state profiles, which correspond to the four marked points in Fig. 5(a), are plotted in Fig. 6. The two steady states obtained for low current densities (square and circle) can be characterized by almost constant ionic strength and negligible electric charge density in the electrolyte bulk. As the voltage increases, the system shifts to the transport limited regime (triangle and diamond). The A^+ ions are the only electric charge carriers at any steady states. A growing supply of electrons to the cathode results in the

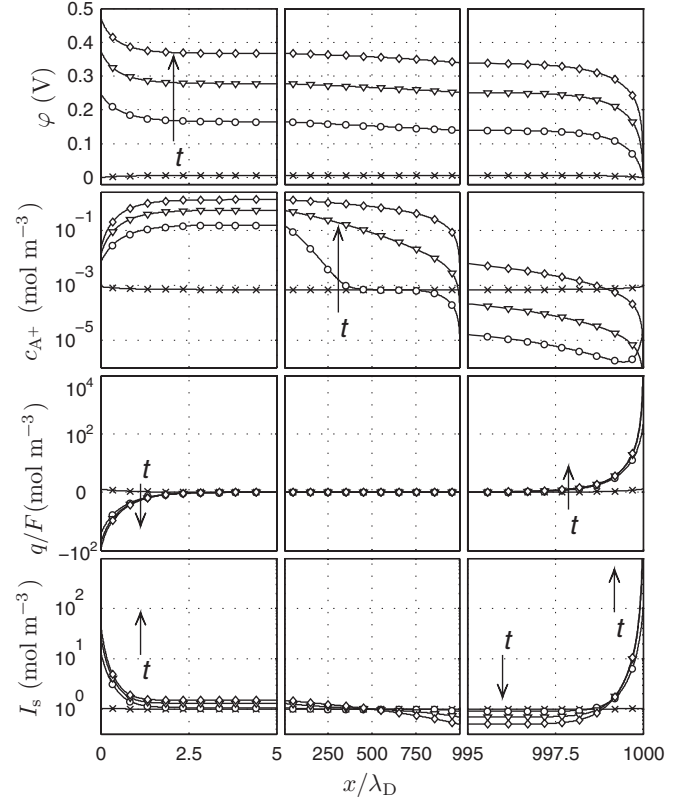


FIG. 4. Transient behavior of the electrochemical cell under a current load ($i = 40 \text{ A m}^{-2}$). Spatial profiles of the electric potential, A^+ concentration, electric charge density, and ionic strength are plotted at four selected times. The diamond-marked profile corresponds to the achieved steady state. The values of the model parameters are $L = 1000\lambda_D$, $k_{\text{red}} = D/\lambda_D^2 \times 10^5 \text{ m}^3 \text{ mol}^{-1}$, $k_{\text{ox}} = D/\lambda_D^2 \times 10^2$, and $K_D = 10(c_0\lambda_D)^2$.

massive formation of the electron donors and in a decrease of the electric potential. The A^+ ions are then intensively consumed on the cathode and simultaneously attracted to the electrode surface from the electrolyte bulk. The electric-field strength in the cathode vicinity becomes high. Hence the other electrolyte components B^- and C^+ are electrostatically expelled from this region and the ionic strength decreases. With growing electric current, the depleted zone extends far from the cathode. A similar phenomenon is observed in the vicinity of ion-exchange membranes under a current load [34].

The obtained CV characteristics of the electrochemical system are in good qualitative agreement with those given by the classical BV theory. A detailed discussion of the compatibility of the proposed kinetic model with the Frumkin modification of BV kinetics is given in Sec. V F.

C. Cyclic voltammetry modeling

We would like to show the capability of our model for cyclic voltammetry modeling. For that reason we have to slightly modify the model. To compute the cyclic voltammetry curves of the whole electrochemical cell we virtually impose a voltage signal $V(t)$ on the system. The corresponding electric current i (an input parameter of the model) can then be simply evaluated as $i = k_i[V(t) - U]$, where U is the difference of the electric

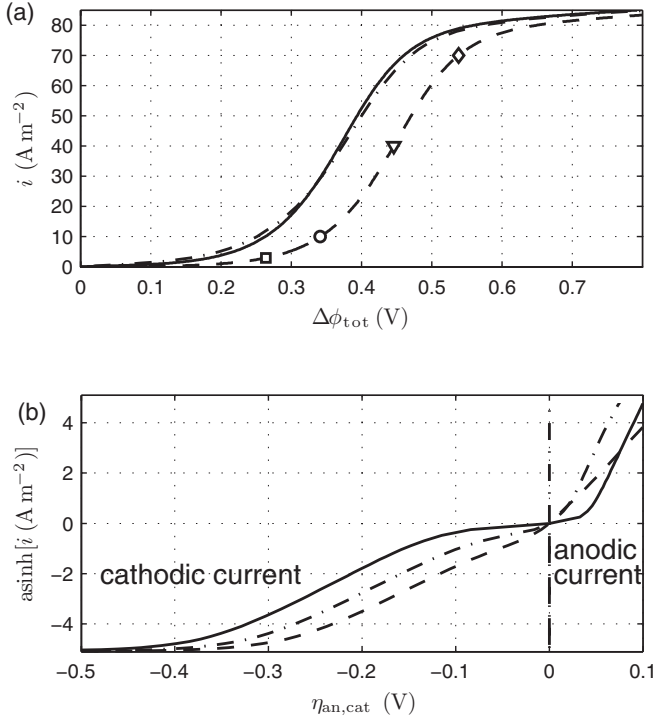


FIG. 5. The CV characteristics of (a) the whole electrochemical cell and (b) half cells. The values of the model parameters are $L = 1000\lambda_D$, $k_{\text{red}} = D/\lambda_D^2 \times 10^2 \text{ m}^3 \text{ mol}^{-1}$, $k_{\text{ox}} = D/\lambda_D^2 \times 10^2$, and $K_D = (c_0\lambda_D)^2$ (dash-dotted line); $L = 1000\lambda_D$, $k_{\text{red}} = D/\lambda_D^2 \times 10^2 \text{ m}^3 \text{ mol}^{-1}$, $k_{\text{ox}} = D/\lambda_D^2 \times 10^2$, and $K_D = 1000(c_0\lambda_D)^2$ (solid line); and $L = 1000\lambda_D$, $k_{\text{red}} = D/\lambda_D^2 \times 10^5 \text{ m}^3 \text{ mol}^{-1}$, $k_{\text{ox}} = D/\lambda_D^2 \times 10^2$, and $K_D = (c_0\lambda_D)^2$ (dashed line).

potential between the two electrodes $\Delta\phi_{\text{tot}}$, $[V(t) - U]$ is the voltage on a virtual resistor between the voltage source and the electrochemical cell, and k_i is a sufficiently high proportionality constant (i.e., a reciprocal resistance of the virtual resistor). To compute the cyclic voltammetry curves of the electrochemical half cell we impose a voltage signal $V(t)$ between the source and the center of the system. Then U is equal to $\Delta\phi_h$.

The data obtained for the whole cell are symmetric due to the reversible chemical reaction and identical composition of the electrodes (Fig. 7). If we plot cyclic voltammetry data for the voltage imposed on a half cell, the symmetry is broken, which manifests different reaction rates of the oxidation and reduction processes. In the corresponding cyclic voltammetry curve, the cathodic and anodic peaks can be simply identified. Although our simulations do not precisely mimic a typical cyclic voltammetry measurement due to the lack of a well-stirred electrolyte bulk, the obtained cyclic voltammetry dependences are in qualitative agreement with the typical shape of cyclic voltammetry curves. We would like to emphasize that our model is able to simulate the entire cyclic voltammograms for fast sweep rates together with the dynamics of the EDL processes. The BV kinetics operates only with electric potential differences between two chosen points of a system [Eqs. (2) and (3)]. The BV approach then does not reveal the real spatial-temporal processes at electrode surfaces.

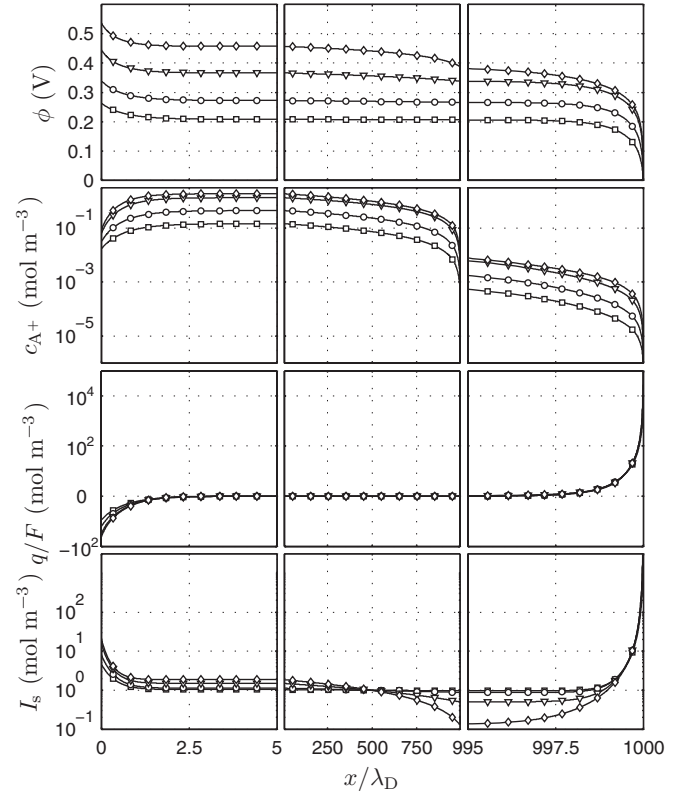


FIG. 6. Stationary behavior of the whole electrochemical cell under a current load for an electric current density of 3 A m^{-2} (squares), 10 A m^{-2} (circles), 40 A m^{-2} (triangles), and 70 A m^{-2} (diamonds). The values of the model parameters are $L = 1000\lambda_D$, $k_{\text{red}} = D/\lambda_D^2 \times 10^5 \text{ m}^3 \text{ mol}^{-1}$, $k_{\text{ox}} = D/\lambda_D^2 \times 10^2$, and $K_D = (c_0\lambda_D)^2$.

D. Nonequilibrium dynamical responses

To highlight the difference in the dynamical behavior (dynamical response) of classical models and our model, we simulate the dynamical response of the proposed model to a fast and symmetric ramplike change of the imposed voltage [Fig. 8(a)]. When the voltage imposed on the electrochemical cell increases [Fig. 8(b)] the concentration of the reactive

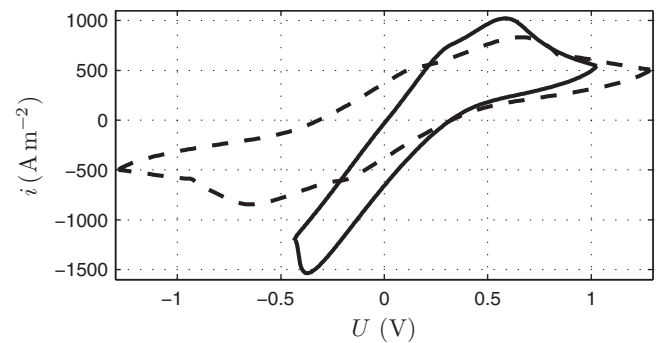


FIG. 7. Cyclic voltammetry simulations: voltage imposed on the whole electrochemical cell $\Delta\phi_{\text{tot}}$ with a sweep rate of 2.78 kV s^{-1} (dashed line) and voltage imposed on one half cell $\Delta\phi_h$ with a sweep rate of 2.22 kV s^{-1} (solid line). The values of the model parameters are $L = 1000\lambda_D$, $k_{\text{red}} = D/\lambda_D^2 \times 10^2 \text{ m}^3 \text{ mol}^{-1}$, $k_{\text{ox}} = D/\lambda_D^2 \times 10^2$, and $K_D = (c_0\lambda_D)^2$ (dashed line) and $L = 1000\lambda_D$, $k_{\text{red}} = D/\lambda_D^2 \times 10^{-3} \text{ m}^3 \text{ mol}^{-1}$, $k_{\text{ox}} = D/\lambda_D^2 \times 10^{-2}$, and $K_D = (c_0\lambda_D)^2$ (solid line).

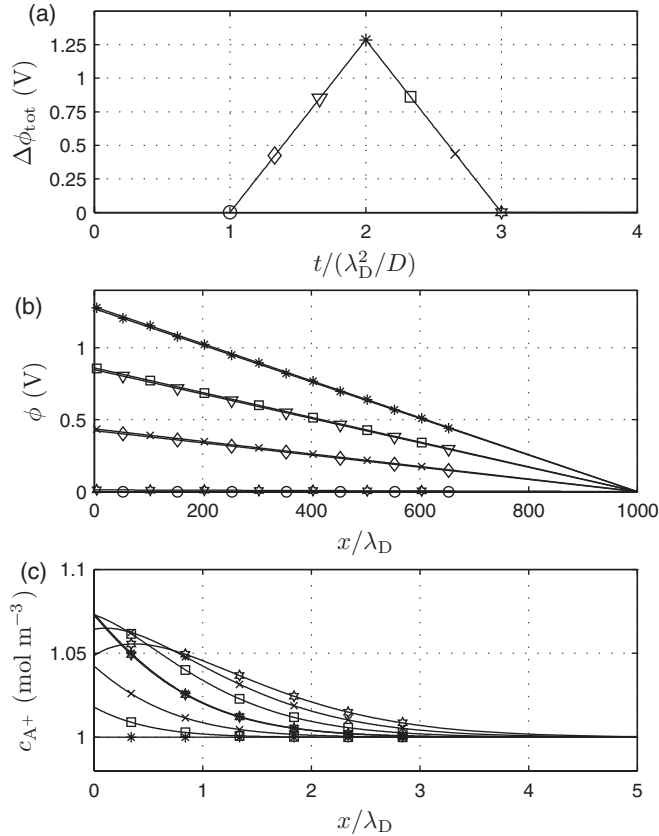


FIG. 8. (a) Ramplike voltage function imposed on the whole electrochemical cell, (b) profiles of the electric potential in the entire cell, and (c) concentration profiles of the reactive ion at the cathode double layer. Markers of the profiles correspond to the marked points on the ramplike function. The model parameters are $L = 1000\lambda_D$, $k_{\text{red}} = D/\lambda_D^2 \times 10^2 \text{ m}^3 \text{ mol}^{-1}$, $k_{\text{ox}} = D/\lambda_D^2 \times 10^2$, and $K_D = (c_0\lambda_D)^2$ and the spatially uniform initial concentrations are $c_{A^+} = 1 \text{ mol m}^{-3}$, $c_{B^-} = 2 \text{ mol m}^{-3}$, and $c_{C^+} = 1 \text{ mol m}^{-3}$.

cation A^+ grows at the cathode [Fig. 8(c)]. The concentration profiles are monotonic at the electrode and similar to the Boltzmann profiles (distributions). If the voltage returns to its origin value, the concentration profiles become nonmonotonic with a concentration maximum at a distance less than one Debye length from the electrode. Such profiles do not satisfy the Boltzmann distribution (equilibrium). This phenomenon occurs when the dynamics of the imposed electric field is so fast that the EDL relaxation time λ_D^2/D is longer than the electric-field dynamics. This aspect is not taken into account in the BV models.

E. Limiting current analysis

We compare predictions of our model with earlier theories for a constant current load [35,36]. For comparison with the models by Ben and Levich, we rescale our model according to Ben's scaling [35]. The voltage is determined as the difference of the electric potential between one electrode and the center of the modeling domain. The parameter l in Ben's model is equal to $500\lambda_D$. The dashed line in Fig. 9 represents Levich's theoretical prediction [Eq. (17)] on the CV response of a uni-

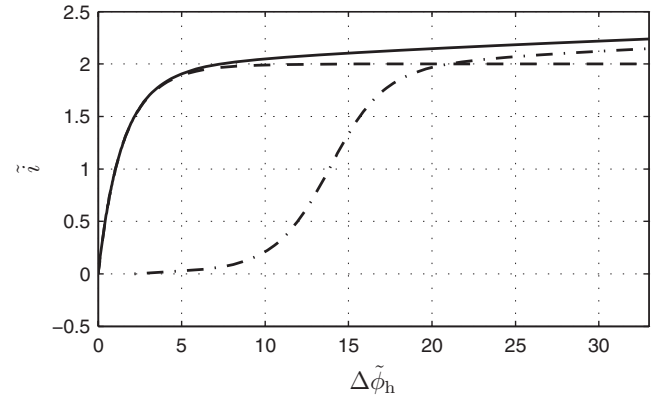


FIG. 9. Current voltage characteristics of the model system in the dimensionless form introduced in Ref. [35] for Levich's prediction (dashed line), our model with three ions (the spatially uniform initial conditions are $c_{A^+} = 0$, $c_{B^-} = 1 \text{ mol m}^{-3}$, and $c_{C^+} = 1 \text{ mol m}^{-3}$) (dash-dotted line), and our model with two ions (the spatially uniform initial conditions are $c_{A^+} = 1 \text{ mol m}^{-3}$ and $c_{B^-} = 1 \text{ mol m}^{-3}$) (solid line). The other model parameters are $L = 1000\lambda_D$, $k_{\text{red}} = D/\lambda_D^2 \times 10^2 \text{ m}^3 \text{ mol}^{-1}$, $k_{\text{ox}} = D/\lambda_D^2 \times 10^2$, and $K_D = (c_0\lambda_D)^2$.

univalent system to the electric current input [36]

$$\tilde{i} = 2\{1 - \exp[-\Delta\tilde{\phi}_h/2 + \ln(p)/2]\}, \quad (17)$$

where p is the surface concentration of the counterions. In our model the surface concentration p depends on the imposed voltage. Hence we determine this concentration from the spatial profile obtained numerically for each imposed $\Delta\tilde{\phi}_h$. One can clearly see the onset of the dimensionless limiting current. Levich's theory predicts a limiting current value equal to 2. The dash-dotted line is obtained by rescaling of our CV characteristic plotted in Fig. 5. Our dependence is characterized by a typical sigmoidal shape with an exponential increase and the reaction limited regime. It differs completely from Levich's dependence; however, the limiting current value is slightly higher than 2 and for higher voltage $\Delta\tilde{\phi}_h \geq 20$ the current increases according to Ben's prediction [35]. First, we introduce the reasons for this apparent discrepancy. In the second step we will show that our model is applicable to Ben's and Levich's problems. Thus we prove the robustness of our model.

In our model we consider the presence of three ions A^+ , B^- , and C^+ . Normally there is a large surplus of nonreactive C^+ ions with respect to the reactive A^+ ions. The negative electric charge accumulated at the electrode surfaces is equilibrated with both the reactive and nonreactive cations. However, only the reactive ion is able to transfer electrons via the electrolyte-electrode boundaries. A relatively low concentration of A^+ leads to a relatively low current response to the imposed voltage or vice versa. To compare the behavior of our model with Ben's and Levich's systems, we considered a zero concentration of the C^+ ion. Then our system behaves as a uni-univalent one. By evolution integration (the imposed electric current was slowly linearly increased with time), we obtain the solid line in Fig. 9. The solid line coincides with Levich's theory for small voltages. For high voltages our model is in agreement with Ben's predictions. Thus our model

is not in disagreement with earlier theoretical models (at least in a steady state) and simultaneously allows us to model more complex nonequilibrium systems.

There are also important works focused on electrochemical systems with a uni-univalent supporting electrolyte that is chemically equivalent to our three-ion system [37,38]. Almog and Yariv derived an asymptotic current-voltage characteristic of a sigmoidal shape [38]. Their result is in qualitative agreement with our findings, which are depicted by the dash-dotted line in Fig. 9. A direct comparison of the models is not possible due to different boundary conditions for the reactive ion.

F. Compatibility of the proposed model with the Frumkin modification of BV kinetics

Our model is in agreement with the Frumkin modification of the BV kinetics [Eq. (3)] at least in low-potential and low-frequency regimes. Under such conditions, the electric potential difference across the Stern layer $\Delta\phi_S$ can be replaced by the surface concentration of the electric charge Q divided by the Stern layer capacitance C_S giving us

$$\frac{i}{F} = k'_O c_A^s \exp\left(\frac{(1-\alpha)FQ}{C_S RT}\right) - k'_R c_{A^+}^s \exp\left(\frac{-\alpha FQ}{C_S RT}\right). \quad (18)$$

When Eqs. (10) and (13) are combined we obtain another expression for the electric current density

$$\frac{i}{F} = k_{\text{ox}}[Q/2F + \sqrt{(Q/2F)^2 + K_D}] - k_{\text{red}c_{A^+}}[-Q/2F + \sqrt{(Q/2F)^2 + K_D}]. \quad (19)$$

Equations (18) and (19) can be rearranged into

$$\frac{i}{F} = k_1 \exp^{k_2 Q} - k_3 \exp^{-k_4 Q}, \quad (20)$$

$$\frac{i}{F} = k_5[k_2 Q + \sqrt{(k_2 Q)^2 + k_6}] - k_7[-k_4 Q + \sqrt{(k_4 Q)^2 + k_8}], \quad (21)$$

where

$$k_1 = k'_O c_A^s, \quad k_2 = \frac{(1-\alpha)F}{C_S RT}, \quad k_3 = k'_R c_{A^+}^s, \quad k_4 = \frac{\alpha F}{C_S RT}, \quad (22)$$

$$k_5 = k_{\text{ox}}/2Fk_2, \quad k_6 = 4F^2 k_2^2 K_D, \quad (23)$$

$$k_7 = k_{\text{red}c_{A^+}}/2Fk_4, \quad k_8 = 4F^2 k_4^2 K_D. \quad (24)$$

In order to obtain the same current density, these conditions have to be satisfied: $k_1 \approx k_5$ and $\exp^{k_2 Q} \approx k_2 Q + \sqrt{(k_2 Q)^2 + k_6}$. Analogously, $k_3 \approx k_7$ and $\exp^{-k_4 Q} \approx -k_4 Q + \sqrt{(k_4 Q)^2 + k_8}$. Now we plot the functions $f(Q) = \exp^{k_2 Q}$ and $g(Q) = k_2 Q + \sqrt{(k_2 Q)^2 + k_6}$ (Fig. 10). Physically relevant values of the constants k_2 and k_6 can be estimated: $F = 96485 \text{ C mol}^{-1}$, $\alpha = 0.5$, $R = 8.314 \text{ J mol}^{-1} \text{ K}^{-1}$, $T = 298 \text{ K}$, $C_S = 1 \text{ F m}^{-2}$ (based on $C_S = \epsilon_S/\lambda_S$, where the Stern layer permittivity and thickness are estimated to be $\epsilon_S = 1 \times 10^{-10} \text{ F m}^{-1}$ and $\lambda_S = 1 \times 10^{-10} \text{ m}$, respectively), and $K_D = 7.1 \times 10^{-14} \text{ mol}^2 \text{ m}^{-4}$. The maximal K_D is estimated

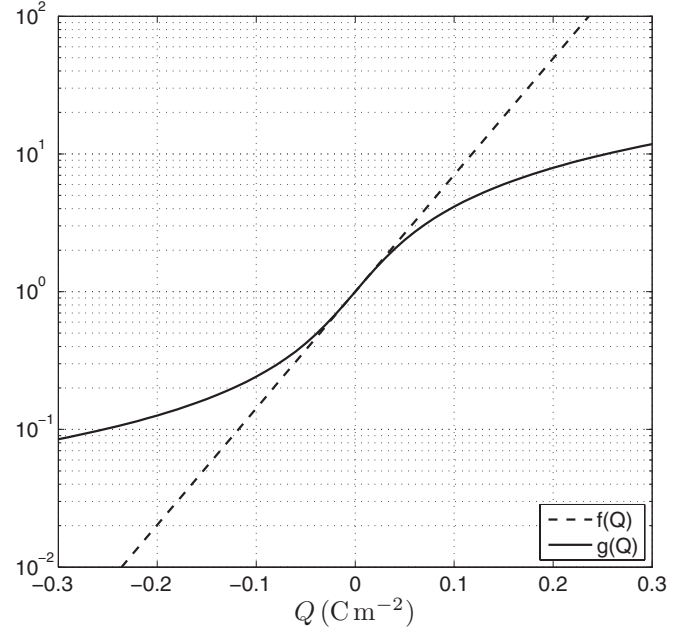


FIG. 10. Plotted functions $f(Q)$ and $g(Q)$ with $k_2 = 19.5 \text{ m}^2 \text{ C}^{-1}$ and $k_6 = 1$.

as the square of surface concentration of the metal atoms on the electrode surface $K_{D,\text{max}} \approx 2.8 \times 10^{-8} \text{ mol}^2 \text{ m}^{-4}$. Our choice of K_D then satisfies our statement about the surplus of the active sites S_{act} . Then the constants k_2 and k_6 are $19.5 \text{ m}^2 \text{ C}^{-1}$ and 1, respectively.

We see that the functions $f(Q)$ and $g(Q)$ perfectly coincide for low values of the electric charge concentration (low differences of the electric potential). There are of course significant discrepancies in regimes with higher electric potential differences. However, the transport of chemical components to the electrode surface becomes the limiting process of the entire system under higher voltages.

VI. CONCLUSION

We believe that the proposed model can be useful for a dynamical analysis of electrochemical microsystems and nanosystems forced by high-frequency electric fields. Our kinetic mechanism also allows one to study and analyze more complex electrochemical systems by simple adding different kinetic terms into the boundary conditions (13).

Our theory allows the description of electrochemical reactions by means of the standard chemical kinetic theory that is widely accepted in chemical reaction engineering. In this theory all concentrations are principally non-negative. Electrons are considered to be reactants in the electrochemical reactions. The introduction of the electron donors and acceptors as reactants then avoids negative electron concentrations.

Moreover, the proposed mechanism allows, in principle, modeling of the electrochemical deposition of metals on a cathode from complex anions (coordination complexes), i.e., the complex anion is split into metal cation and other anions. This happens at the electric double layer, where the electric-field strength is high enough to split the complex anion. We have no idea how to describe this process by the BV kinetics.

ACKNOWLEDGMENTS

The authors are grateful for support from the GAAV ČR (Grant No. IAA401280904), the Ministry of Education, Youth and Sports of the Czech Republic (Grants No. 6046137306 and No. 21/2012).

APPENDIX: DIMENSIONLESS MODEL

The model equations are transformed into a dimensionless form. The spatial coordinate x is scaled by the Debye length λ_D

$$\tilde{x} = \frac{x}{\lambda_D}, \quad (\text{A1})$$

where the Debye length can be written as

$$\lambda_D^2 = \frac{\varepsilon RT}{2 c_0 F^2}. \quad (\text{A2})$$

The dimensionless time \tilde{t} is given by

$$\tilde{t} = \frac{t}{t_0}, \quad t_0 = \frac{\lambda_D^2}{D}. \quad (\text{A3})$$

The other dimensionless quantities are defined by

$$\tilde{c}_i = \frac{c_i}{c_0}, \quad \tilde{\phi} = \frac{\phi}{\phi_0}, \quad \phi_0 = \frac{RT}{F}, \quad \tilde{q} = \frac{q}{q_0}, \quad q_0 = F c_0. \quad (\text{A4})$$

The Poisson equation in the dimensionless form is given by

$$\frac{\partial^2 \tilde{\phi}}{\partial \tilde{x}^2} = -\tilde{q} = -\sum_i z_i \tilde{c}_i \quad (\text{A5})$$

and the molar balances of ions are

$$\frac{\partial \tilde{c}_i}{\partial \tilde{t}} = -\frac{\partial}{\partial \tilde{x}} \left(-\frac{\partial \tilde{c}_i}{\partial \tilde{x}} - z_i \tilde{c}_i \frac{\partial \tilde{\phi}}{\partial \tilde{x}} \right). \quad (\text{A6})$$

The dimensionless surface concentrations of acceptors, donors, and electric charge are defined as

$$\tilde{c}_{A^+} = \frac{c_{A^+}}{c_{E0}}, \quad \tilde{c}_{D^-} = \frac{c_{D^-}}{c_{E0}}, \quad \tilde{Q} = \frac{Q}{Q_0}, \quad (\text{A7})$$

where

$$c_{E0} = c_0 \lambda_D, \quad Q_0 = F c_0 \lambda_D, \quad j_0 = \frac{c_0 D}{\lambda_D}. \quad (\text{A8})$$

Then we can write

$$\tilde{c}_{A^+} = \left(\tilde{Q} + \sqrt{\tilde{Q}^2 + \frac{4K_{AD}}{(c_0 \lambda_D)^2}} \right) / 2, \quad (\text{A9})$$

$$\tilde{c}_{D^-} = \left(-\tilde{Q} + \sqrt{\tilde{Q}^2 + \frac{4K_{AD}}{(c_0 \lambda_D)^2}} \right) / 2. \quad (\text{A10})$$

Equations (13) and (14) take the form

$$\tilde{J}_{A^+} \Big|_{\tilde{x}=0, L/\lambda_D} = \frac{\lambda_D^2}{D} (k_{\text{ox}} \tilde{c}_{A^+} - k_{\text{red}} c_0 \tilde{c}_{A^+} \tilde{c}_{D^-}), \quad (\text{A11})$$

$$\frac{\partial \tilde{Q}_A}{\partial \tilde{t}} \Big|_{\tilde{x}=0} = \tilde{i} - \frac{\lambda_D^2}{D} (k_{\text{ox}} \tilde{c}_{A^+} - k_{\text{red}} c_0 \tilde{c}_{A^+} \tilde{c}_{D^-}), \quad (\text{A12})$$

$$\frac{\partial \tilde{Q}_C}{\partial \tilde{t}} \Big|_{\tilde{x}=L/\lambda_D} = -\tilde{i} - \frac{\lambda_D^2}{D} (k_{\text{ox}} \tilde{c}_{A^+} - k_{\text{red}} c_0 \tilde{c}_{A^+} \tilde{c}_{D^-}). \quad (\text{A13})$$

The dimensionless electric current is introduced as

$$\tilde{i} = \frac{i}{i_0}, \quad i_0 = \frac{F c_0 D}{\lambda_D}. \quad (\text{A14})$$

The electric potential boundary conditions and the initial conditions in dimensionless form are

$$\tilde{\phi} \Big|_{\tilde{x}=L/\lambda_D} = 0, \quad \frac{\partial \tilde{\phi}}{\partial \tilde{x}} \Big|_{\tilde{x}=0} = -\tilde{Q}, \quad (\text{A15})$$

$$\tilde{c}_{B^-, C^+} \Big|_{\tilde{x}, \tilde{t}=0} = 1, \quad \tilde{c}_{A^+} \Big|_{\tilde{x}, \tilde{t}=0} = 0. \quad (\text{A16})$$

-
- [1] M. Ni *et al.*, *J. Power Sources* **163**, 460 (2006).
 [2] O. Marina *et al.*, *J. Electrochem. Soc.* **154**, B452 (2007).
 [3] R. O'Hayre *et al.*, *Fuel Cell Fundamentals* (Wiley, New York, 2006).
 [4] D. Linden, *Handbook of Batteries* (McGraw-Hill, New York, 1995).
 [5] B. Wang *et al.*, *J. Electrochem. Soc.* **143**, 3204 (1996).
 [6] J. Bates *et al.*, *Solid State Ion.* **135**, 33 (2000).
 [7] H. Uhlig, *Corrosion and Corrosion Control* (Wiley, New York, 1971).
 [8] K. Vetter, *Electrochemical Kinetics* (Academic, New York, 1967).
 [9] L. H. Olesen, H. Bruss, and A. Ajdari, *Phys. Rev. E* **73**, 056313 (2006).
 [10] A. Ramos *et al.*, *J. Colloid Interface Sci.* **309**, 323 (2007).
 [11] P. Červenka *et al.*, *IEEE Trans. Ind. Appl.* **46**, 1679 (2010).
 [12] J. Hrdlička, P. Červenka, M. Příbyl, and D. Šnita, *Phys. Rev. E* **84**, 016307 (2011).
 [13] A. Zelinsk and B. Pirogov, *Electrochim. Acta* **54**, 6707 (2009).
 [14] M. Svoboda *et al.*, *Microelectron. Eng.* **86**, 1371 (2009).
 [15] T. E. Gruz *et al.*, *Z. Phys. Chem. A* **150**, 203 (1930).
 [16] A. Frumkin, *Z. Phys. Chem. A* **164**, 121 (1933).
 [17] G. Brug *et al.*, *J. Electroanal. Chem.* **176**, 275 (1984).
 [18] D. Harrington *et al.*, *Electrochim. Acta* **32**, 1703 (1987).
 [19] O. Azizi *et al.*, *Int. J. Hydrogen Energy* **32**, 1755 (2007).
 [20] B. Conway *et al.*, *Electrochim. Acta* **31**, 1013 (1986).
 [21] D. Schönfuss *et al.*, *Electrochim. Acta* **39**, 2097 (1994).
 [22] W. D. Murphy *et al.*, *J. Phys. Chem.* **96**, 9983 (1992).
 [23] A. A. Moya *et al.*, *J. Phys. Chem.* **99**, 1292 (1995).
 [24] A. Bonnefont *et al.*, *J. Electroanal. Chem.* **500**, 52 (2001).
 [25] M. Z. Bazant *et al.*, *SIAM J. Appl. Math.* **65**, 1463 (2005).
 [26] R. He *et al.*, *J. Phys. Chem. B* **110**, 3262 (2006).
 [27] P. Biesheuvel *et al.*, *Electrochim. Acta* **54**, 4857 (2009).
 [28] M. Soestbergen, *Electrochim. Acta* **55**, 1848 (2010).
 [29] M. van Soestbergen, P. M. Biesheuvel, and M. Z. Bazant, *Phys. Rev. E* **81**, 021503 (2010).
 [30] D. Lastochkin *et al.*, *J. Appl. Phys.* **96**, 1730 (2004).

- [31] Z. Gagnon *et al.*, *Electrophoresis* **26**, 3725 (2005).
- [32] L. Ejlsing, K. Smistrup, C. M. Pedersen, N. A. Mortensen, and H. Bruus, *Phys. Rev. E* **73**, 037302 (2006).
- [33] J. O. Bockris, A. K. N. Reddy, and M. Gamboa-Aldeco, *Modern Electrochemistry 2A* (Kluwer Academic Publishers, New York, 2000).
- [34] T. Postler *et al.*, *J. Colloid Interface Sci.* **320**, 321 (2008).
- [35] Y. Ben and H. C. Chang, *J. Fluid Mech.* **461**, 229 (2002).
- [36] V. G. Levich, *Physicochemical Hydrodynamics* (Prentice-Hall, Englewood Cliffs, NJ, 1962).
- [37] E. Yariv and Y. Almog, *Phys. Rev. Lett.* **105**, 176101 (2010).
- [38] Y. Almog and E. Yariv, *Phys. Rev. E* **84**, 041204 (2011).